



UNIVERSITÀ POLITECNICA DELLE MARCHE
Repository ISTITUZIONALE

Delamination buckling of GFRP-strips in strengthened RC beams

This is the peer reviewed version of the following article:

Original

Delamination buckling of GFRP-strips in strengthened RC beams / Capozucca, R.; Magagnini, E.; Bettucci, E.. - In: COMPOSITE STRUCTURES. - ISSN 0263-8223. - STAMPA. - 300:(2022).
[10.1016/j.compstruct.2022.116183]

Availability:

This version is available at: 11566/305561 since: 2024-04-26T12:22:04Z

Publisher:

Published

DOI:10.1016/j.compstruct.2022.116183

Terms of use:

The terms and conditions for the reuse of this version of the manuscript are specified in the publishing policy. The use of copyrighted works requires the consent of the rights' holder (author or publisher). Works made available under a Creative Commons license or a Publisher's custom-made license can be used according to the terms and conditions contained therein. See editor's website for further information and terms and conditions.

This item was downloaded from IRIS Università Politecnica delle Marche (<https://iris.univpm.it>). When citing, please refer to the published version.

(Article begins on next page)

Delamination buckling of GFRP-strips in strengthened RC beams

by

R. Capozucca¹, E. Magagnini², E. Bettucci³

ABSTRACT

Fiber Reinforced Polymer (FRP) strips are convenient materials in the strengthening of damaged RC beams of bridges due to corrosion or impact loading and in the rehabilitation of RC beams damaged by seismic actions. The behaviour of Externally Bonded (EB) FRP strips has been extensively studied when the strengthening is subjected to tensile stresses, even if, in many cases, due to cyclic actions, FRP strips glued to the concrete surface may be subjected to compression. Compressive stresses on the FRP strip may cause a buckling mechanism with detachment.

In this work, an investigation of reinforced concrete (RC) beam models undamaged and damaged and strengthened with GFRP strips on compressive and tensile sides is shown. Beam models were subjected to four-point bending tests and the delamination buckling mechanism of the GFRP strip has been described. Further, analytical models to study the delamination buckling of strengthening with FRP strips are developed. Finally, experimental and theoretical data are discussed.

Keywords: RC Beam; Damage; FRP; Bending tests; Delamination buckling.

¹ Full Prof. of Struct. Engineering, Struct. Section DICEA, Università Politecnica delle Marche, Ancona, ITALY, phone +39.071.2204570 fax +39.071.2204576 r.capozucca@staff.univpm.it

² PhD, DICEA, Università Politecnica delle Marche, Ancona, ITALY e.magagnini@staff.univpm.it .

³ PhD student, DICEA, Università Politecnica delle Marche, Ancona, ITALY, e.bettucci@pm.univpm.it

1. Introduction

In recent years there has been an increase in the use of composite materials for strengthening of damaged structural elements such as reinforced concrete (RC) beams under loading; nodes of columns and beams of frames and cross walls of buildings damaged by seismic actions. Further, usually, prestressed RC beams of bridges must be strengthened for the increase of service loads or damages due to impact loadings. In this regard, the deterioration of structural elements subjected to environmental chemical agents like pollution or consequences of an unforeseen state of local damage due to both impact loading and corrosion of steel reinforcement is becoming an emerging duty of research in civil engineering. In general, strengthening with external bonded (EB) Fiber Reinforced Polymer (FRP) strips glued on the concrete surface may be an efficient way to increase the stiffness and strength of damaged RC structures. This technique is based on the maintenance of FRP strip bonded without delamination and detachment until the ultimate strain capacity of compressive concrete. The loss of bond is often due to several failure modes observed in numerous experimental studies [1-4]: flexural failure by loss of tensile capacity of FRP strips; intermediate flexural cracks; concrete cover separation; etc. [5]. Many failure modes with debonding of FRP strips glued to concrete surface happen on the tensile side.

Although the EB FRP strips are mainly used for strengthening on the tensile side, under cyclic loading as seismic actions, FRP strips may be subjected to a compressive state of loading [6-8] that may lead to FRP strip delamination for critical compressive loads and buckling. In many cases, the phenomenon of delamination buckling is underestimated although the loss of strengthening may cause a loss of the strength of the hybrid system or a decrease in the capacity of strengthening.

Although Externally Bonded Reinforcement (EBR) is a common method for mounting the sheet that uses conventional surface preparation, in recent years Grooving Method (GM) in its special form of Externally Bonded Reinforcement On Grooves (EBROG) has been proposed as an alternative to the conventional method of surface preparation in EBR method [9], with the aim to postpone or totally prevent such buckling.

51 On delamination buckling, works have been developed to analyze laminated plates by thin-film model
52 with analytical delamination models, since 1981 by Chai [10]. Other researchers derived formulas for
53 thin-film strips in composite laminates [11] and analyzed the deformation of the delaminated
54 composite under axial loading including shear effects [12]. The growth of delamination under
55 constant amplitude of cyclic compression has been studied in composite plates by Kardomateas et al.
56 [13]. Reddy et al. [14] have developed a theory to account for multiple delaminations between layers.
57 An analytical model to predict delamination buckling of FRP strip in a reinforced timber beam has
58 been presented as a civil engineering problem of rehabilitation of structural elements by Kim et al.
59 [15]. This model has been utilized below to study the mechanism of delamination of GFRP strip in
60 the strengthening of RC beams under bending tests.

61 In addition, analytical and experimental studies to investigate delamination post-buckling behaviour
62 of thin plates constrained to a rigid element [16] or compressive buckling of plates in unilateral
63 contact [17] are reported in the literature. Effects of the delamination taking into account shear-
64 deformable bilayer beam theory [18,19] and analysis of buckling loads for unsymmetric flat laminates
65 subjected to biaxial compression and shear loads resting on elastic foundations have been developed
66 [20]. In the last decades, computational models using Finite Elements (FE) have been proposed by
67 many authors [21-23]. Numerical modellings based on the virtual crack closure technique [24,25],
68 and cohesive zone model [26,27] have been assessed to simulate and predict the onset and the
69 propagation of delamination buckling in a composite structure.

70 Unfortunately, most existing studies focused on the response of a delaminated thin laminate without
71 a relevant effect on the strength of hybrid elements; few studies and investigations are carried out on
72 the delamination buckling mechanism of FRP strips glued to RC beams damaged as strengthening
73 [7,8,28]. The mechanism of delamination buckling has been noted also in the strengthening with
74 GFRP strips of cross-damaged masonry walls [6,29].

75 In the following, hybrid systems such as RC beam models strengthened with EB FRP strips are
76 investigated by bending laboratory tests. The availability of strengthening and the maintenance of

bond of FRP strips subjected to compressive loading has been experimentally analyzed and the mechanism of loss of adhesion due to delamination buckling is also studied with analytical modelling. In a hybrid system as RC beam with FRP strips, materials are bounded with a layer of adhesive and the loss of adhesion may cause delamination at the interface of adherents [30,31]. In the case of an RC beam reinforced with FRP on the compression surface of concrete, the debonding of the FRP strip can carry out consequences on the capacity of the hybrid system for the deflection of beam. Local instability decreases suddenly the availability of strengthening with interlayer crack and separation of the FRP layer from the concrete surface. In this paper, an investigation of two RC beam models damaged and undamaged, strengthened with GFRP strips both on the compressive and tensile side, subjected to four-point bending is shown. The beam models have been assumed with initial damage by a notch. The presence of damage as localized notch may be representing a concentrated damage due to impact or local effect of corrosion of steel reinforcement and consequent reduction of the strength capacity of concrete. So, the choice to damage the RC beam models by notching came from the purpose to investigate the effect of localized damage with a high reduction of global stiffness and to control the availability of bond of GFRP strip on both upper and lower side of beam models. It was chosen to adopt GFRP strips as strengthening because the aim of the experimental tests was not to have a strengthening of high mechanical properties but to control the delamination mechanism even when using reinforcement of lower capacity and therefore the highest resistance values are not reached.

Analytical models, formulated under different assumptions, are described to predict bending loading of delamination buckling of GFRP strips in strengthened RC beams as appropriately as possible and results of experimental tests and analytical models are compared and discussed.

2. Experimental bending tests

2.1. RC beam models and set-up for bending tests

Static experimental tests were carried out on three RC beam models named A0, A and B with the same geometric characteristics. The dimensions of the beam sections were 80mm·120mm and measured 1100mm in length. The steel reinforcement used was 4 bars with a diameter 6mm, two in tension and two in compression and vertical stirrups at 50-100 mm intervals having a diameter of 6mm (Fig. 1(a) and (b)). The average yielding stress of steel bars was $f_y \geq 500$ N/mm² and Young's modulus equal to $E_s = 2.1 \cdot 10^5$ N/mm², as declared by the manufacturer. The main parameters of tested beams are summarized in Table 1.

Furthermore, the steel reinforcement has been designed to obtain a scale model compared to the full-scale one, which guarantees failure by bending and not by shear. In the experimental tests, two RC beam models have been artificially damaged by notches at midspan. The two RC beam models are studied with two different degrees of damage linked to the width and position of notches: in the first beam, type A, 10 mm of the concrete cover was removed from the upper surface; in the second one, type B, it was chosen to remove the concrete cover all around the midspan for a width of 15mm (Fig. 2(a) and (b)).

The beam model, labelled as A0, was used as an undamaged beam. Once damaged, the two RC beams were repaired by filling notches with thixotropic mortar. After strengthening with mortar filled in the notches, the two RC beams are reinforced with EB GFRP strips that are bounded to the beam through a biphasic epoxy resin. The epoxy resin, adopted as the matrix, is characterized by the following mechanical properties: Young's modulus $E_{res} = 1600$ N/mm² and Poisson's modulus $\nu_{res} \approx 0.48$, obtained by compression tests on two prismatic specimens. Two GFRP strip specimens of thickness about $t_{GFRP} = 1.2$ mm were experimentally subjected to tension according to the ASTM-D 3039 Standard [32]. The dimension of specimens subject to tensile tests and data recorded by experimentation are summarized in Table 2.

128 The two RC beams were strengthened with externally bonded EB GFRP strips glued on the tensile
129 and compression sides of the concrete surface (Fig. 3). Beam type A was strengthened with externally
130 bonded EB GFRP strips glued on the tensile side, for a length of 1000 mm, and on the compressive
131 side of the concrete surface, for a length of 300 mm, with a width of 50 mm, as shown in Figure 3(a).
132 Beam type B was strengthened with externally bonded EB GFRP strips glued on the tensile and
133 compressive sides of the concrete surface for a length of 300 mm with a width of 50 mm (Fig. 3(b)).
134 After the strengthening with GFRP strips, the beams were tested by bending loading until failure with
135 control of displacement. For the execution of the four-point bending test, two hinges with a wheelbase
136 of 1000 mm and two loads with a wheelbase of 300 mm arranged symmetrically to the centerline
137 were arranged. The tests' setup is shown in Figure 4(a).

138 The experimental response of the damaged beams strengthened with GFRP strips under bending load
139 has been compared with that obtained for the undamaged condition (beam A0), to evaluate the actual
140 capacity of GFRP strips to improve the performance of damaged beams.

141 Static tests were performed to verify the availability of GFRP strengthening in the tensile and
142 compressive zone and to monitor possible local mechanisms of delamination.

143 Beam models A0, A and B were subjected to cyclic increasing load equal to 3.0kN, 8.0kN, 12.0kN.
144 After these cycles of loading, beam A0 was subjected to bending until failure; while beams A and B
145 have been strengthened by GFRP strips and subjected again to increasing load until failure.

146 The beams were tested in hinge-hinge end condition by a specific steel support system. The
147 instruments used in the static tests were a vertical jack to transmit the load $2F$ with a load cell to
148 measure the entity of load and two strain gauges (E1 and E2) to record deformation during bending
149 tests, one on the compressive side and one on the tensile side of beams (Fig. 4(b)). In addition to the
150 instruments described above, two horizontal linear transducers (LVDTs 1 and 2) to record
151 deformation on each lateral surface of compressed concrete (Fig. 4(b)) were adopted.

152

153

154 2.2. Experimental results

155 The main results obtained during the static bending tests are summarized in Table 2 where the loading
156 degree by bending is shown as D_i^* with $i=1,2,3$.

157 The collapse of beam A0 happened at a load value equal to $2F \cong 15.77\text{kN}$; the maximum experimental
158 measured value of compressed concrete strain was equal to $\varepsilon_c \cong 2.77 \cdot 10^{-3}$. The failure was due to the
159 crash of the concrete's compressive edge.

160 Figure 5 shows the development of cracking damage in strengthened beam type A for each load value.
161 To complete the test, the beam has been subjected to bending up failure, which occurred for a load of
162 about $2F \cong 23\text{ kN}$ (Fig. 6). Further damage recurs from a load of 15 kN and tends to increase. Figure
163 6(a) shows the damage for loads exceeding 9 kN. Detailed damage of the EB GFRP strip is also
164 shown in Figure 6(b), where we can also see the beginning of delamination buckling, which happened
165 at about 21 kN.

166 The failure of beam type B occurred at a load value equal to $2F \cong 15\text{kN}$, caused by the complete
167 detachment of the GFRP strip for delamination buckling at the compressive side and successively
168 expulsion of the concrete cover at the tensile side with the GFRP strip's detachment. Figure 7 shows
169 the development of cracking damage in strengthened beam type B. The typical GFRP strips'
170 detachment due to delamination buckling under bending tests of beam model B is shown in Figure 8.
171 Experimental diagrams of load ($2F$) versus strains at midspan for beams A and B are shown in Figures
172 9 and 10.

173 After damage degree D^*3 , the strain gauge E1 (Fig. 4(b)), positioned on the GFRP strip at the
174 compressive side of the beam, was no longer able to provide measurements due to the start of the
175 delamination buckling process (Figs. 9 and 10).

176 The envelope of experimental diagram moment, M , versus curvature, χ , for each tested beam,
177 evaluated considering the strains on the compressed concrete surface of midspan section (or on
178 compressive GFRP strip) and tensile GFRP strip, is shown in Figure 11.

179 The first aspect that needs to be stressed is the effect of the GFRP strengthening system on the
180 structural response of each RC beam. For beam type A, with EB GFRP strips placed at the
181 compressive side for a length of 300mm and at the tensile side for the entire length, it can be noticed
182 how the strengthening by EB GFRP equipped beam led to an increase in the moment capacity of a
183 reinforced concrete flexural member, equal to about 29% concerning A0 capacity. For beam type B,
184 with EB GFRP strips placed at the compressive and tensile sides for a length of 300mm, the increase
185 in resistance is absent; due mainly to a failure mechanism that involved the delamination buckling of
186 GFRP at the compressive side, the expulsion of the concrete cover at the tensile side with the
187 detachment of the tensile GFRP strip and the high concentration of intermediate cracks along the
188 filled notch at mid-span section with the formation of local cracking mechanisms.

189 From the analysis of the behaviour of the GFRP strip under compression, in both cases investigated,
190 it is possible to state that the presence of the strengthening on the compressive side allows having a
191 reinforcement also on the upper surface, which still works but is conditioned by the delamination
192 buckling. After the beginning of the debonding of the GFRP strip, there is an increase equal to about
193 10% and 20%, respectively, for beam types A and B, of the moment that the beams can withstand
194 before failure (Fig. 11).

195 What is mainly observed in both cases investigated is that GFRP strips allow an increase of the strain
196 capacity under loading, conferring to the strengthened RC beams, a good level of ductility under
197 bending, with values of ductility ratio deduced by the ratio of ultimate curvature value, χ_u , on yield
198 curvature, χ_y , greater than $\chi_u/\chi_y > 1.5$, for both cases investigated (Fig. 11).

199 Another aspect that needs to be underlined is the influence of the local concentrated damage on the
200 structural response of the system. For beam type B, the presence of a deep notch with the removal of
201 the concrete cover all around the midspan section represents a very strong and deep weakening in a
202 zone where the maximum moment acts. The damage by deep notch leads to a substantial loss of
203 stiffness, which is not recovered by the consolidation by mortar. In this case, the strengthening by EB
204 GFRP allows an increase of the deformation capacity under loading although the stiffness of the beam

205 is on the whole smaller, as it is possible to verify by the diagrams moment versus curvature for the
206 tested beam models in Figure 11. For beam type A, where the notch is positioned only on the upper
207 surface of the beam at the midspan section, the effect of damage in terms of loss of stiffness is limited,
208 as confirmed by Figure 11.

209 Furthermore, it can be observed that, from results obtained by experimental bending tests, the
210 delamination buckling mechanism could be affected by local damage; this is confirmed by the
211 analysis of failure modes of GFRP strengthened beams that do not include any concrete layer but just
212 adhesive interface, as shown in Figure 8. Nevertheless, the delamination buckling mechanism is not
213 necessarily activated in the section where the notch is placed, as can be seen in Figure 6(b). If we
214 analyse the values of the moment and curvature for which the instability mechanism is activated (Fig.
215 11), it can be noted that in the case of notch concentrated on the upper surface (beam type A), the
216 beginning of delamination buckling is recorded for a level of the moment that is 75% higher than in
217 the case of notch positioned all around the midspan (beam type B), with almost equal curvature
218 values.

219

220 **3. Theoretical buckling load for FRP strip**

221 In the following, analytical models are described to analyse the mechanism of delamination buckling.
222 Analytical simulation is certainly quite complex. However, theoretical models will be discussed, in
223 which the FRP strip is considered both as a slender beam without adhesion and as an element on an
224 elastic medium represented by the adhesive. In this way, theoretical and experimental results can be
225 discussed and analyzed as appropriately as possible.

226

227 **3.1. FRP thin strip as slender beam**

228 The following differential equation may be used to describe the deflection of a layer of GFRP
229 subjected to delamination in a composite beam (Fig. 12):

$$230 \quad w'' = -\frac{M}{EI} + \left(\frac{V}{GA_v}\right)' \quad (1)$$

231 when:

$$232 \quad M'' = -q_z ; \quad V = M' \quad (2)$$

233 where: E is the Young's modulus; $G = \frac{E}{2(1+\nu)}$ the shear modulus with ν = Poisson ratio; A the cross

234 section area; $A_v = \alpha_v A$ the shear area; α_v = area shear factor and I the moment of inertia related to

235 the principal axis of the section. In Eq. (1) the w'' is increased by $\left(\frac{V}{GA_v}\right)'$, which represents the

236 contribution of shear in the differential equation for a bar element under bending. The effect of shear

237 deformations can be considered as a generalization of the Timoshenko beam when the problem of

238 delamination buckling of a thin layer of FRP glued to a surface of the RC beam is studied.

239 Considering a local delamination buckling of FRP strip as shown in Figure 12, the governing Eq. (1)

240 with Eq. (2) may be written as:

$$241 \quad w'' = -\frac{M}{EI} + \frac{M''}{GA_v} \quad (3)$$

242 The equilibrium permits to write (Fig. 12(b))

$$243 \quad M' = V + P \cdot w' \quad (4)$$

244 where P is the compression force on the FRP layer supposed constant. Finally, from derivation of Eq.

245 (3) we obtain:

$$246 \quad w^{IV} = -\frac{M''}{EI} + \frac{Pw^{IV}}{GA_v} \quad (5a)$$

247 then:

$$248 \quad EIw^{IV} \left(1 - \frac{P}{GA_v}\right) + Pw'' = 0 \quad (5b)$$

$$249 \quad w^{IV} + \frac{P}{EI \left(1 - \frac{P}{GA_v}\right)} \cdot w'' = 0 \quad (5c)$$

250 The equation (5c) is the governing equation for the top layer of FRP under buckling. Assuming b the

251 width and t_{FRP} the thickness of the FRP layer, the value of $A_v = \frac{5}{6}b \cdot t_{FRP}$ can be obtained. If we

252 introduce a coefficient:

$$253 \quad \alpha^2 = \frac{P}{EI \left(1 - \frac{P}{GA_v}\right)} = \frac{P}{EI \left(1 - \frac{1.2P}{G \cdot b \cdot t_{FRP}}\right)} \quad (6)$$

254 the general solution of (5c) may be expressed as:

255 $w(x) = C_1 + C_2 \cdot x + C_3 \cos \alpha x + C_4 \sin \alpha x$ (7)

256 By the symmetry of the layer's deformation, the solution is:

257 $w(x) = C_1 + C_3 \cos \alpha x$ (8)

258 Considering $a = l/2$, the boundary conditions at $x = a$ permit to obtain the non-trivial solution as

259 $\sin(\alpha a) = 0$. The lowest value of the solution is $\alpha a = n\pi$ for $n = 1$ with $\alpha^2 = \frac{\pi^2}{a^2}$. Considering

260 equation (6) we obtain [33]:

261 $P_{cr,T} = \frac{P_{cr,E}}{\left(1 + \frac{1.2P_{cr,E}}{G \cdot b \cdot t_{FRP}}\right)}$ (9)

262 with $P_{cr,E} = \pi^2 \frac{EI}{a^2}$ the Euler's load.

263

264 **3.2. FRP strip as a beam on an elastic medium**

265 The following analysis of delamination buckling of FRP strip has been developed using a model

266 which considers the normal stresses in interfacial due to adhesive as an equivalent elastic beam. The

267 assumptions are: all materials are linear as in the above analysis of stress distribution; the plan sections

268 remain plane after delamination buckling; the bond between adhesive and FRP strip remains up to

269 the displacement of FRP due to delamination buckling. In Figure 13 the deflection of the compressed

270 FRP strip is shown with the adhesive layer assuming plane. The FRP strip is assumed as an elastic

271 beam glued to the adhesive layer, of unknown length l .

272 The interfacial normal stress in the adhesive can be expressed as follows:

273 $\sigma_n(x) = K_n \cdot w_a(x)$ (10)

274 in which K_n is the normal stiffness of the adhesive on unit length. It can be written as:

275 $K_n(x) = \frac{\sigma_n(x)}{w_a(x)} = \frac{E_a}{t_a}$ (11)

276 being

277 $w_a(x) = w(x)$ (12)

278 with $w_a(x)$ the normal displacement of adhesive between the interface FRP strip and adhesive.

279 We consider that elastic constant K_0 is the value $K_0 = K_n \cdot b$, being b width of FRP. The distribution
280 of normal load on unit length may be expressed as:

$$281 \quad p(x) = (K_n \cdot b) \cdot w(x) \quad (13)$$

282 Based on principal work, it is possible to write:

$$283 \quad \frac{P}{2} \cdot \int w'^2(x) dx = \frac{1}{2} \int K_0 w^2(x) dx + \frac{1}{2} \int EI w''^2(x) dx \quad (14)$$

284 Following Rayleigh's procedure, it is possible to assume a function, $w(x)$, for the shape:

$$285 \quad w(x) = w_0 \sin \pi \frac{x}{l} \quad (15)$$

286 and substitute it in Eq. (14) and solve for P which is the critical buckling load for delamination
287 buckling.

288 The final expression may be obtained:

$$289 \quad \frac{P}{2} \cdot \left(\frac{\pi}{l}\right)^2 \cdot w_0^2 \cdot \frac{l}{2} = \frac{1}{2} K_0 \cdot w_0^2 \cdot \frac{l}{2} + \frac{1}{2} EI \cdot \left(\frac{\pi}{4}\right)^4 \cdot w_0^2 \cdot \frac{l}{2} \quad (16)$$

290 and

$$291 \quad P_{cr,FRP} = K_0 \cdot \left(\frac{l}{\pi}\right)^2 + EI \cdot \left(\frac{\pi}{l}\right)^2 \quad (17)$$

292 Eq. (17) says that $P_{cr,FRP}$ is greater than the Euler load, which is augmented $K_0 \cdot \left(\frac{l}{\pi}\right)^2$ due to the
293 adhesive layer.

294 Assuming $\beta = \sqrt[4]{\frac{K_0}{4EI}}$ it is possible to write:

$$295 \quad \frac{P_{cr}}{\sqrt{K_0 EI}} = t^2 + \left(\frac{1}{t}\right)^2 \quad (18)$$

296 with t a dimensionless coefficient equal to:

$$297 \quad t = \frac{\sqrt{2}}{\pi} \cdot \beta \cdot l \quad (19)$$

298 and for $t = 1$:

$$299 \quad P_{cr} = 2 \cdot \sqrt{K_0 EI} \quad (20)$$

300 which is the smallest load of delamination buckling for any length l . We obtain for the length the

following value:

$$l = \frac{\pi}{\sqrt{2}} \cdot \frac{1}{\beta} = \pi \cdot \sqrt[4]{\frac{EI}{K_0}} \quad (21)$$

4. FRP strip on the compressive side of RC beam under bending

We consider an RC beam under bending test with delamination buckling of FRP which is symmetric about the mid-span (Fig. 14(a)). The displacement, rotation and force acting are computed considering displacement functions, evaluated with boundary conditions for each segment of the beam [15] as shown in Appendix A.

For the equilibrium of segments 1 and 2 and the compatibility of the axial displacement between segments 2 and 3, we can obtain rotation values, θ , of the section at the beginning of the delaminated section ($x_2 = -\frac{l}{2}$). Equalizing rotation values, a relationship between the normal force P and the bending load F can be written:

$$F = \frac{P \cdot h}{(L-L_0)} - \frac{4D_2}{l(L-L_0)} \cdot \left[\frac{3h}{l} - \sqrt{\frac{9h^2}{l^2} + 6P \left(\frac{1}{A_2} + \frac{1}{A_3} \right)} \right] \quad (22)$$

where the stiffnesses $D_2 = (EI)_2$, $A_2 = (EA)_2$ and $A_3 = (EA)_3$ are relative to segments 2 and 3 of the beam.

Then introducing the expression of the load P_{cr} leading to the mechanism of delamination by instability in Eq. (22), the force F_{cr} can be evaluated by the same Eq. (22) which is valid up to the condition of stability.

5. Discussion

Strengthening with EB GFRP strips on the compression side of RC beam highlighted the possible local instability phenomenon of the glued strip. The adoption of analytical models to study the delamination buckling mechanism of the GFRP strip under compression allows calculating the value of critical load corresponding to the beginning of delamination. However, these theoretical models

are suitable for calculating the value of the critical load in case of symmetrical problems, when FRP is symmetric about the mid-span, as shown in Figures 12, 13 and 14.

In first approximation, can be evaluated by considering Euler's formula of instability of FRP strip as a beam with shear stiffness with reference to Timoshenko beam. The theoretical curves of load, $P_{cr,E}$, and $P_{cr,T}$, versus delamination length, l , are shown in Figure 15(a). Since the thickness of the GFRP strip is one of uncertain parameter, Figure 15(a) shows the curves varying the thickness of the GFRP strip, $t_{GFRP} = 1.0 - 1.2 - 1.5$ mm. The critical load P_{cr} may be compared with an estimated value from experimental tests. The strain values along the GFRP strip on the beam's compressive side recorded experimentally at the beginning of the delamination mechanism, are equal to about $\varepsilon \cong 3.9 \cdot 10^{-3}$, for the type A beam, and $\varepsilon \cong 5.69 \cdot 10^{-3}$ for the type B beam. Taking the average value of strain, $P_{cr} = E_{GFRP} \cdot \varepsilon \cdot A_{GFRP} \cong 15$ kN for $t_{GFRP} = 1$ mm, so the delamination length may be assumed between 10÷25mm.

The analytical model shown above for the beam subjected to bending tests permits us to obtain the relationship (22), between P_{cr} and the corresponding force F_{cr} . Eq. (22) can be simplified as follows:

$$F_{cr} = \frac{P_{cr} \cdot h}{(L - L_0)} \quad (23)$$

Theoretical diagrams of critical force, F_{cr} , vs delamination length, l , are shown in Figure 15(b), varying the GFRP strip's thickness.

Considering experimental results as shown for the two beams, type A and type B, in Figures 9 and 10, the field of delamination length may be restricted to 10÷15mm like the portion of the diagram in Figure 15(b) varying the thickness of the GFRP strip, between $t_{GFRP} = 1.0$ and $t_{GFRP} = 1.5$ mm. Figure 15(b) highlights the values' range of delamination length for various values of GFRP thickness, t_{GFRP} , considered as impregnated. Obviously, it is not correct to experimentally measure the length l of the delaminated section because the mechanism is sudden; therefore, we can refer to the experimental load values that fall within the theoretical limits indicated in Fig 15(b).

350 By Eq. (20), it is possible to estimate the elastic constant value, K_0 , for the delamination length range
351 $10 \leq l \leq 15$ mm and the corresponding P_{cr} values (Fig. 15(a)).
352 Values of normal stiffness of the adhesive on unit length, K_n , versus the thickness of the GFRP strip
353 are shown in Table 4.

354

355 **6. Conclusions**

356 This paper deals with the analysis of delamination buckling of GFRP strips externally bounded on
357 RC beams, damaged with different notches. Three different analytical models were presented to
358 discuss the delamination buckling mechanism affecting GFRP bounded on a concrete surface and to
359 analyze the experimental results as completely as possible. The main results obtained are:

- 360 - analysis of the GFRP strip's behaviour under compression in two RC beams carried out with
361 two RC beam models under bending test until failure has shown the mechanism of
362 delamination buckling with reduction of the strengthening availability;
- 363 - although the strengthening with GFRP strip is conditioned by the phenomenon of
364 delamination, the strengthening with GFRP strip of damaged RC beams with different notches
365 allows to obtain an increase in ductility;
- 366 - the comparison of analytical and experimental results values of the critical load, F_{cr} , permits
367 to evaluate the delamination length range between 10 ± 15 mm;
- 368 - values of K_0 , which represents the actual contribution of the adhesive to the maintenance of
369 stability, have been evaluated in the same delamination length range.

370

371 **Acknowledgement**

372 This experimental research was supported by research funds provided by Università Politecnica delle
373 Marche. The authors would like to express their gratitude to all the technicians and students who
374 collaborated to develop the experimental research.

375

376

377 Appendix A

378 It is described below the analytical model developed by [15] and adopted in Section 4 to describe the
379 mechanism of delamination buckling of GFRP strip under compression in the strengthening of RC beams
380 under bending tests.

381 In the segment between the hinge A and the applied force F, considering three segments (Fig. 14(a)) of the
382 beam under bending, $0 < x_1 < \left(\frac{L}{2} - \frac{L_0}{2}\right)$, moment varies linearly; the displacement function $w_1(x_1)$, as a
383 polynomial of the 3rd degree, can be assumed considering for $x_1 = 0 \rightarrow w_1 = 0$:

$$384 \quad w_1(x_1) = ax_1^3 + bx_1^2 + cx_1 \quad (A1)$$

385 Then:

$$386 \quad M(x_1) = -(EI)_1 w_1'' = F \cdot x_1 \quad (A2)$$

387 and:

$$388 \quad V(x_1) = F = -w_1''' = 6a \quad (A3)$$

389 The a, b coefficients of (A1) may be determined by the boundary condition:

$$390 \quad a = -\frac{F}{6(EI)}; b = 0 \quad (A4)$$

391 and the function of deflection in segment 1 is:

$$392 \quad w_1(x_1) = -\frac{F}{6(EI)_1} \cdot x_1^3 + cx_1 \quad (A5)$$

393 For the evaluation of displacement relative to segment 2, with constant moment $(-\frac{l}{2} < x_2 < 0)$, a displacement
394 function is assumed:

$$395 \quad w_2(x_2) = ex_2^2 + fx_2 + g \quad (A6)$$

396 Indicating with δ and θ the values of displacement and rotation of the section at the beginning of the
397 delaminated section ($x_2 = -\frac{l}{2}$) and being $(fx_2) \cong 0$ by symmetry, we obtain:

$$398 \quad \begin{cases} \delta = e \left(\frac{l}{2}\right)^2 + g \\ \theta = -2a \frac{l}{2} \end{cases} \quad (A7)$$

399 and then the constants are determined by the values of δ and θ :

$$400 \quad e = -\frac{\theta}{l}; g = \delta + \theta \frac{l}{4} \quad (A8)$$

401 Then, the function of deflection $w_2(x_2)$ is expressed as:

$$402 \quad w_2(x_2) = -\frac{\theta}{l} x_2^2 + \left(\delta + \theta \frac{l}{4}\right) \quad (A9)$$

403 In the part relative to segment 1, between the point of force application and the beginning of FRP strip
404 delamination, $(\frac{L}{2} - \frac{L_0}{2} < x_1 < \frac{L}{2} - \frac{l}{2})$, the displacement function can be expressed as:

$$405 \quad w_1(x_1) = a_1 x_1^2 + b_1 x_1 + c_1 \quad (A10)$$

406 Being $-(EI)_1 \cdot w_1''(x_1) = M(x_1)$, from which for $\bar{x}_1 = \left(\frac{L}{2} - \frac{L_0}{2}\right)$ the value of the moment is equal to $M(\bar{x}_1) =$
407 $\frac{F}{2}(L - L_0)$. Then, coefficients a_1 and b_1 can be determined and they are equal to:

$$408 \quad \begin{cases} a_1 = -\frac{F}{4(EI)_1} \cdot (L - L_0) \\ b_1 = \frac{F}{4(EI)_1} \cdot (L - L_0) \cdot (L - l) + \theta \end{cases} \quad (A11)$$

409 Finally, for $\bar{x}_1 = \frac{L}{2} - \frac{l}{2} \rightarrow w_1(\bar{x}_1) = d$, considering Eqs. (A10) and (A11), the expression of c_1 is also obtained.

410 Displacement function (A10) can be written as:

$$411 \quad w_1(x_1) = \left[-\frac{F}{4(EI)_1} \cdot (L - L_0)\right] \cdot x_1^2 + \left[\frac{F \cdot (L - L_0) \cdot (L - l)}{4(EI)_1} + \theta\right] \cdot x_1 + \delta - \left(\frac{L - l}{2}\right) \theta - \frac{F \cdot (L - L_0) \cdot (L - l)^2}{16(EI)_1} \quad (A12)$$

The evaluation of the displacement function for the part of FRP subject to post-buckling shape is given by the solution of the differential equation (5b) relative to a part of length l with stiffness $(EI)_{FRP}$. Considering Eq. (8) and the boundary conditions of the interface between segments 1 and 3, we obtain:

$$\begin{cases} C_1 + C_2 \cos \alpha x|_{x=l} = \delta \\ -\alpha C_2 \sin \alpha x|_{x=l} = \theta \end{cases} \quad (A13)$$

Therefore:

$$C_2 = -\frac{\theta}{\alpha \sin(\alpha l)} ; C_1 = \delta + \frac{\theta}{\alpha} \cdot \frac{\cos \alpha l}{\sin \alpha l} \quad (A14)$$

from which:

$$w_3(x_3) = \left[\delta + \frac{\theta}{\alpha} \operatorname{ctg}(\alpha l) \right] - \frac{\theta}{\alpha \sin(\alpha l)} \cdot \cos \alpha x_3 \quad (A15)$$

In Figure 14(b) segments 1 and 2 are in equilibrium, so we can write:

$$M_1 = (M_2 + \Delta M_2) \cong M_2 + P \cdot \frac{h}{2} \quad (A16)$$

neglecting the thickness of the FRP strip.

The moment-curvature relations for M_1 and M_2 , neglecting the possible cracking of the strained concrete, are:

$$M_1 = -D_1 \frac{d^2 w_1}{dx_1^2} = \frac{F(L-L_0)}{2} \quad (A17)$$

$$M_2 = -D_2 \frac{d^2 w_2}{dx_2^2} = -D_2 \frac{2\theta}{l}$$

considering Eqs. (A9) and (A12). Using Eqs. (A16) and (A17), θ can be expressed as:

$$\theta = \frac{l}{4D_2} \cdot [F(L-L_0) - Ph] \quad (A18)$$

For the compatibility of the axial displacement between segments 2 and 3, we obtain:

$$\frac{P}{A_3} l = \frac{1}{2} \int_{-\frac{l}{2}}^{\frac{l}{2}} \left(\frac{dw_2}{dx_2} \right)^2 dx_2 + h\theta - \frac{P}{A_2} l \quad (A19)$$

where A_2 and A_3 are the axial stiffnesses of, respectively, segments 2 and 3.

Then, the value of angle θ has been obtained as it follows:

$$\theta = -\frac{3h}{l} + \sqrt{\frac{9h^2}{l^2} + 6\left(\frac{P}{A_2} + \frac{P}{A_3}\right)} \quad (A20)$$

From Eqs. (A17) and (A19) we obtain a relationship between normal force P and the bending load F :

$$F = \frac{P \cdot h}{(L-L_0)} - \frac{4D_2}{l(L-L_0)} \cdot \left[\frac{3h}{l} - \sqrt{\frac{9h^2}{l^2} + 6P\left(\frac{1}{A_2} + \frac{1}{A_3}\right)} \right] \quad (A21)$$

where the stiffnesses $D_2 = (EI)_2$, $A_2 = (EA)_2$ and $A_3 = (EA)_3$ are relative to segments 2 and 3 of the beam.

442 **NOTATION**

443	f_y	= yield strength of steel reinforcements
444	E_s	= Young's modulus of steel reinforcements
445	E_{res}	= Young's modulus of epoxy resin
446	ν_{res}	= Poisson's coefficient of epoxy resin
447	t_{GFRP}	= thickness of GFRP strip
448	f_{GFRP}	= tensile strength of GFRP strip
449	E_{GFRP}	= Young's modulus of GFRP strip
450	b	= width of GFRP strip
451	L_0	= length of GFRP strip on compression side
452	A_{GFRP}	= cross section area of GFRP strip
453	L	= length of beam
454	h	= height of beam
455	B	= width of beam
456	f_c	= compressive strength of concrete
457	E_c	= Young's modulus of concrete
458	I	= moment of inertia of beam
459	D^*_i	= damage degree for cracking of concrete
460	ε_c	= strain of compressive concrete
461	ε_{ct}	= strain of tensile concrete
462	ε_{GFRP}	= strain of GFRP
463	M	= bending moment
464	χ	= curvature
465	c, t	= index for compression and tensile side of beams
466	F	= applied force
467	P	= compression load
468	$P_{cr,E}$	= critical Euler compression load
469	$P_{cr,T}$	= critical Timoshenko compression load
470	t_{FRP}	= thickness of the FRP layer
471	F_{cr}	= applied force that leads to instability mechanism
472	K_0	= elastic constant of adhesive
473	K_n	= normal stiffness of adhesive on unit length
474	l	= delamination length of GFRP strip
475	G	= shear modulus
476	α_v	= area shear factor
477	A_v	= shear area
478	$w_a(x)$	= normal displacement of adhesive
479	E_a	= Young's modulus of adhesive
480	t_a	= thickness of adhesive
481	$p(x)$	= distribution of normal load on unit length
482	$\sigma_n(x)$	= interfacial normal stress in the adhesive

483
484
485
486
487
488
489
490
491

493 **References**

- 494 1. An W, Saadatmanesh H, Ehsani MR. RC beams strengthened with FRP plates. II: analysis and
495 parametric study. *J. Struct Eng* 1991; 117(11): 3434–3455.
- 496 2. Plevris N, Triantafillou T.C. Strengthening of RC beams with epoxy-bonded fibre composite
497 materials. *Mater Struct* 1992; 25: 201–211.
- 498 3. Malek AM, Saadatmanesh H, Ehsani MR. Prediction of failure load of RC beams strengthened
499 with FRP plate due to stress concentration at the plate end. *ACI Struct J* 1998; 95(1): 142–152.
- 500 4. Chajes M.J., Thomson Jr T.A., Januszka T.F., Finch Jr WW. Flexural strengthening of concrete
501 beams using externally bonded composite materials. *Constr Build Mater* 1994;8(3): 131-201.
- 502 5. Smith S.T., Teng J.G. FRP strengthened RC beams-I: review of debonding strength models.
503 *Eng. Structures* 2002; 24(4).
- 504 6. Capozucca R., Magagnini E., Experimental response of masonry walls in-plane loading
505 strengthened with GFRP strips. *Comp Struct*, 2020, 235, 111735.
- 506 7. Capozucca R., Magagnini E., Vecchiotti M.V. Delamination Buckling of FRP: Experimental
507 Tests and Theoretical Model. In: Wahab M. (eds) *Proceedings of the 13th International*
508 *Conference on Damage Assessment of Structures (DAMAS 2019)*, Porto, Portugal, 9-10 July
509 2019, *Lecture Notes in Mechanical Engineering*. Springer, Singapore, 2020, 753-766.
- 510 8. Capozucca R. Double-leaf masonry walls under in-plane loading strengthened with
511 GFRP/SRG strips. *Eng. Struct.*, 2016, 128: 453-473.
- 512 9. Mostofinejad D., Moghaddas A., Bond efficiency of EBR and EBROG methods in different
513 flexural failure mechanisms of FRP strengthened RC beams. *Construct Build Mater*, 2014; 54:
514 605-614.
- 515 10. Chai H., Babcock C.D., Knauss W.G. One dimensional modelling of failure in laminated plates
516 by delamination buckling. *Int. J. Solid Struct.* 1981; 17(11): 1069-1083.
- 517 11. Yiu W.L. The effects of laminated structure on delamination buckling and growth. *J.*
518 *Composite Mater.* 1988; 22(6): 502-517.
- 519 12. Kardomateas G.A., Schmueser D.W. Buckling and postbuckling of delaminated composites
520 under compressive loads including transverse shear effects. *AIAA J.* 1988; 26(3): 337-343.
- 521 13. Kardomateas G.A., Pelegri A.A., Malik B. Growth of internal delaminations under cyclic
522 compression in composite plates. *J. Mech Phys Solids* 1995; 43(6): 847-868.
- 523 14. Reddy J.N., Barbero E. J., Teply J.L. A plate bending element based on a generalized laminate
524 plate theory. *Int. J. Numerical Meth. Eng.* 1989; 28: 2275-2292.
- 525 15. Kim Y, Davalos JF, Barbero EJ. Delamination buckling of FRP layer in laminated wood
526 beams. *Compos Struct* 1997; 37(3–4): 311–320.
- 527 16. Chai H. Contact buckling and post buckling of thin rectangular plates. *J. Mech. Phys. Solids*
528 2001; 49: 209-230.
- 529 17. Ma X., Butterworth J.W., Clifton C. Compressive buckling analysis of plate in unilateral
530 contact. *Int. J. Solids Struct.* 2007; 44: 2852-2862.
- 531 18. Qiao P., Wang J. Mechanism and fracture of crack tip deformable bi-material interface. *Int. J.*
532 *Solids Struct.* 2004; 41: 7423-7444.

19. Qiao P., Shan L., Chen F., Wang J. Local delamination buckling of laminated composite beams using novel joint deformation models. *J. Eng. Mech.* 2010; 136: 541-550.
20. Aiello M.A., Ombres L. Buckling and vibrations of unsymmetric laminates resting on elastic foundations under in-plane and shear forces. *Composite Structures*, 1999, 44(1): 31-41.
21. Lampani, L. Finite element analysis of delamination of a composite component with the cohesive zone model technique. *Engineering Computations*, 2011, 28(1): 30-46.
22. Gaudenzi P. On delamination buckling of composite laminates under compressive loading. *Composite Structures*, 1997, 39(1-2): 21-30.
23. Gaudenzi P., Perugini P., Riccio A. Post-buckling behavior of composite panels in the presence of unstable delaminations. *Composite Structures*, 2001, 51: 301-309.
24. Krueger R. Virtual crack closure technique: history, approach, and applications. *Applied Mechanics Reviews*, 2004, 57(2): 109-143.
25. Gasco F., Feraboli P. A crack length control scheme for solving nonlinear finite element equations in stable and unstable delamination propagation analysis. *Composite Structures*, 2014, 117: 267-273.
26. De Borst R. Numerical aspects of cohesive-zone models. *Engineering Fracture Mechanics*, 2003, 70: 1743-1757.
27. Harper P.W., Hallett S.R. Cohesive zone length in numerical simulations of composite delamination", *Engineering Fracture Mechanics*, 2008, 75: 4774-4792.
28. Capozucca R., Magagnini E. RC beam models damaged and strengthened with GFRP strips under bending loading and free vibration. *Comp Struct*, 2020, 253, 112730.
29. Capozucca R. Vibration analysis of damaged RC beams strengthened with GFRP. *Composite Structures*, 2018, 624-634.
30. L. M. Kachanov, *Delamination Buckling of Composite Materials. Mechanics of Elastic Stability*, vol 14. Springer, Dordrecht, 1988.
31. Mei H., Huang R., Chung J.Y., Stafford C.M., Yu H.H. Buckling modes of elastic thin films on elastic substrates. *Appl. Phys. Lett.*, 2007, 90 (15): 151902.
32. ASTM D 3039/D3039M-08. Tensile Properties of Polymer Matrix Composite Materials, in *Annual Book of ASTM: Composite Materials*; 2008.
33. Peter Marti. *Theory of structures: fundamentals, framed structures, plates and shells*. Wilhelm Ernst & Sohn, 2013, Berlin.

List of Figures:

- Figure 1 RC beam models: (a) cross section and (b) longitudinal section with steel bars and stirrups.
- Figure 2 Damages in RC beam models: (a) first beam - type A; (b) second beam - type B.
- Figure 3 RC beam strengthened with GFRP: (a) beam type A and (b) beam type B.
- Figure 4 (a) Set up of static bending tests; (b) instruments to measure strain at midspan section.
- Figure 5 Cracking damage development due to bending for beam A with GFRP strips.
- Figure 6 (a) Damage development at $2F=21\text{kN}$ for beam type A with GFRP strips; (b) delamination buckling.
- Figure 7 Cracking damage development due to bending for beam B with GFRP strips.
- Figure 8 Detail of delamination buckling of beam type B.
- Figure 9 Exp. diagram load, $2F$, vs strain of GFRP strip, $\varepsilon_{GFRP,C}$ at the compressive side of beam A.
- Figure 10 Exp. diagram load, $2F$, vs strain of GFRP strip, $\varepsilon_{GFRP,C}$, at the compressive side of beam B.
- Figure 11 Comparison between experimental moment, M , vs. curvature, χ , diagrams.
- Figure 12 (a) Local delamination buckling of FRP strip; (b) internal action.
- Figure 13 Deflection of compressed FRP strip.
- Figure 14 (a) RC beam under bending experimental test; (b) RC beam with FRP delaminated.
- Figure 15 (a) Theoretical diagrams $P_{cr,E}$, $P_{cr,T}$, vs delamination length, l and (b) theoretical diagrams F_{cr} , vs delamination length, l , for different values of GFRP thickness, t_{GFRP} , of strip.

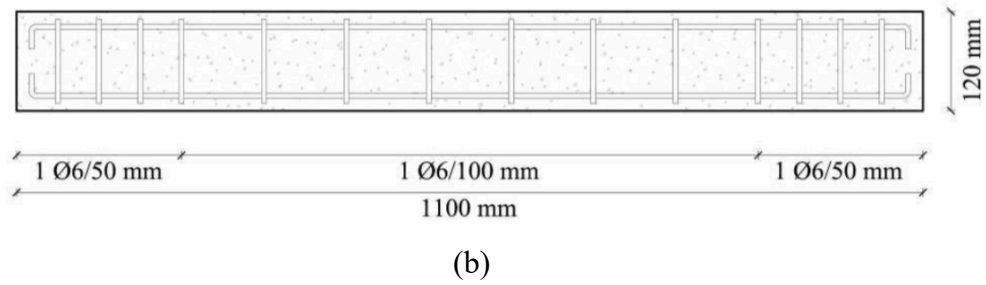
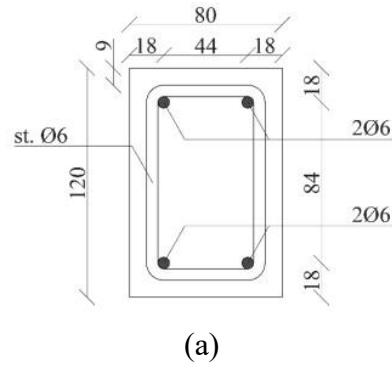


Figure 1 – RC beam models: (a) cross section and (b) longitudinal section with steel bars and stirrups.

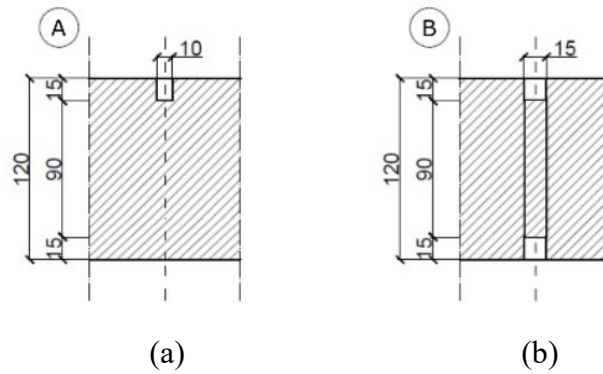


Figure 2 – Damages in RC beam models: (a) first beam - type A; (b) second beam - type B.

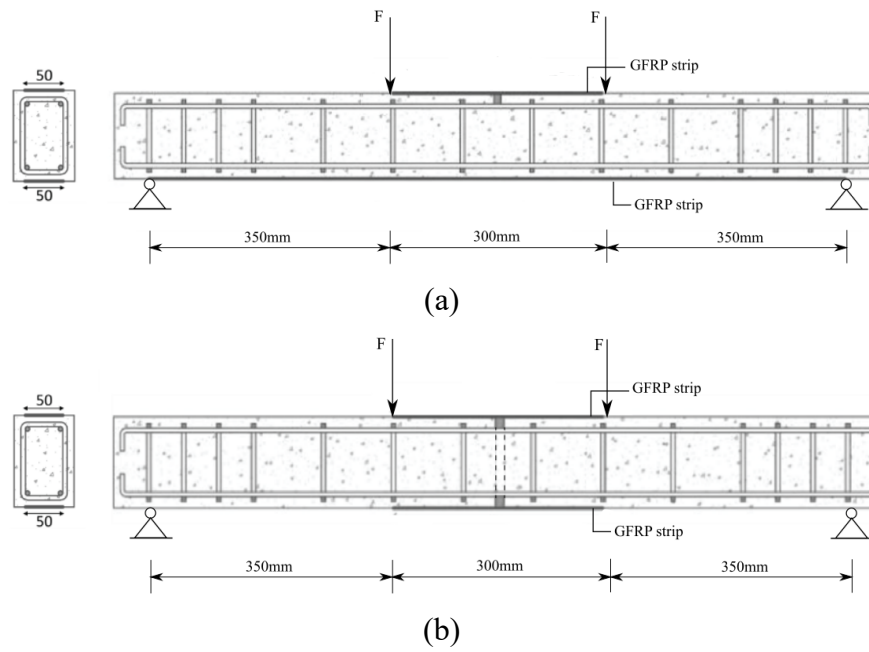


Figure 3 – RC beam strengthened with GFRP: (a) beam type A and (b) beam type B.

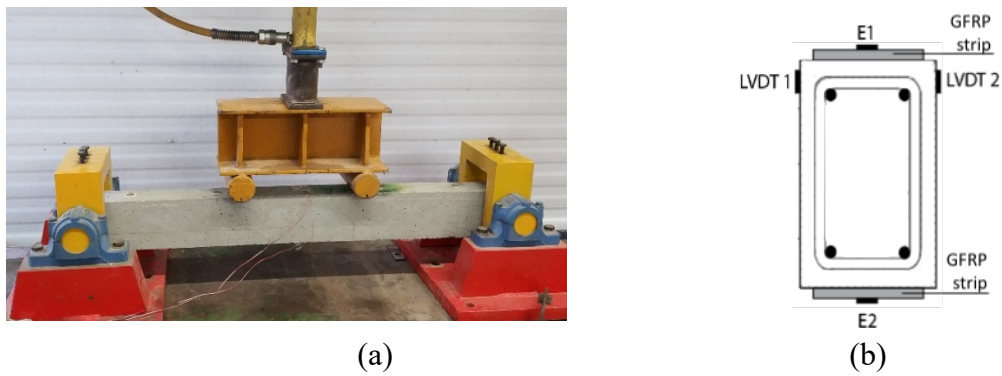
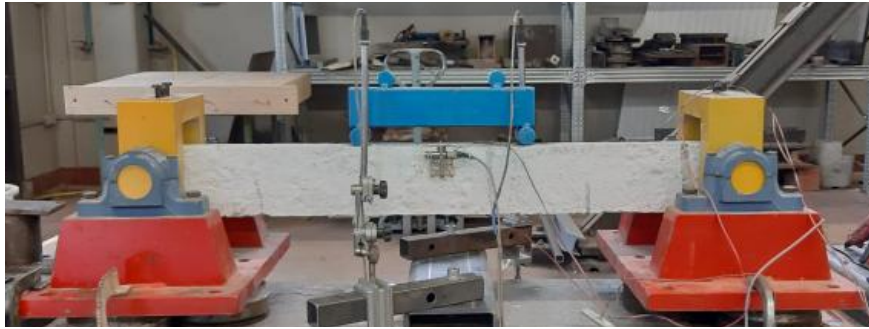
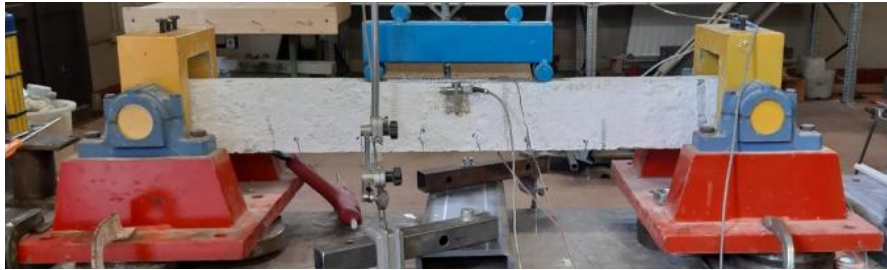


Figure 4 – (a) Set up of static bending tests; (b) instruments to measure strain at midspan section.



$2F = 3\text{kN}$

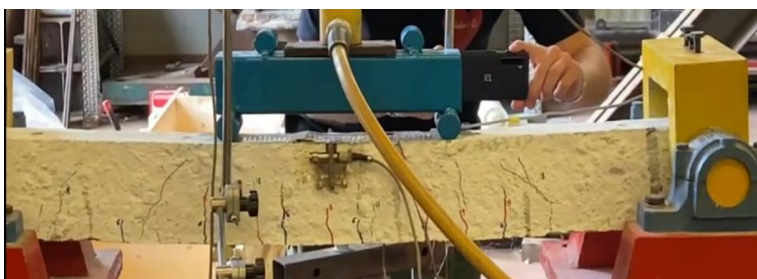


$2F = 6\text{kN}$



$2F = 9\text{kN}$

Figure 5 – Cracking damage development due to bending for beam A with GFRP strips.

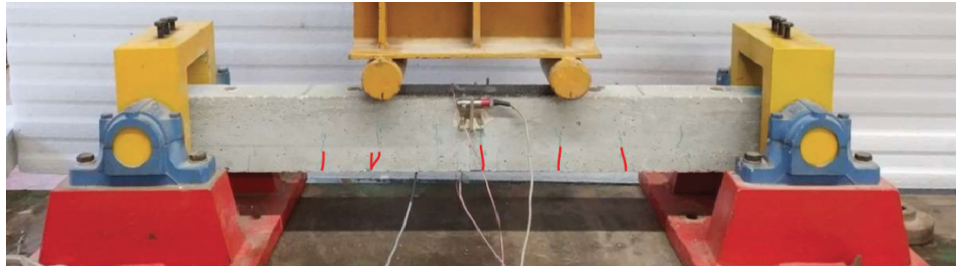


(a)

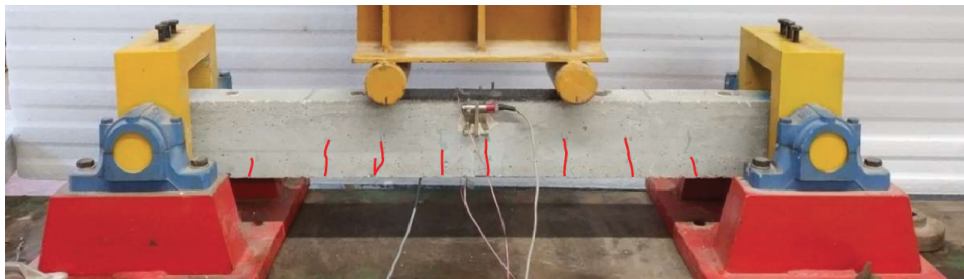


(b)

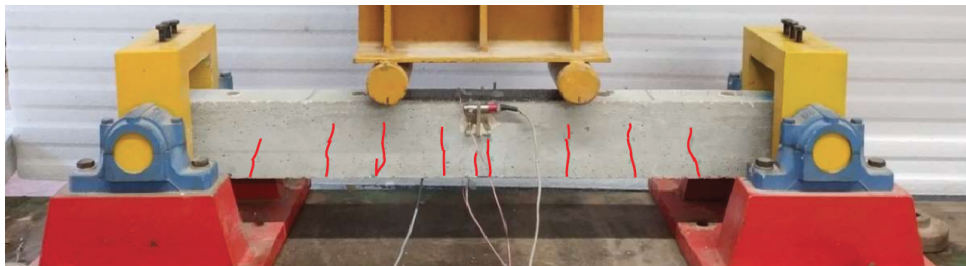
Figure 6 – (a) Damage development at $2F = 21\text{kN}$ for beam type A with GFRP strips; (b) delamination buckling.



$2F = 4\text{kN}$



$2F = 8\text{kN}$



$2F = 12\text{kN}$

Figure 7 – Cracking damage development due to bending for beam B with GFRP strips.



Figure 8 – Detail of delamination buckling for beam type B.

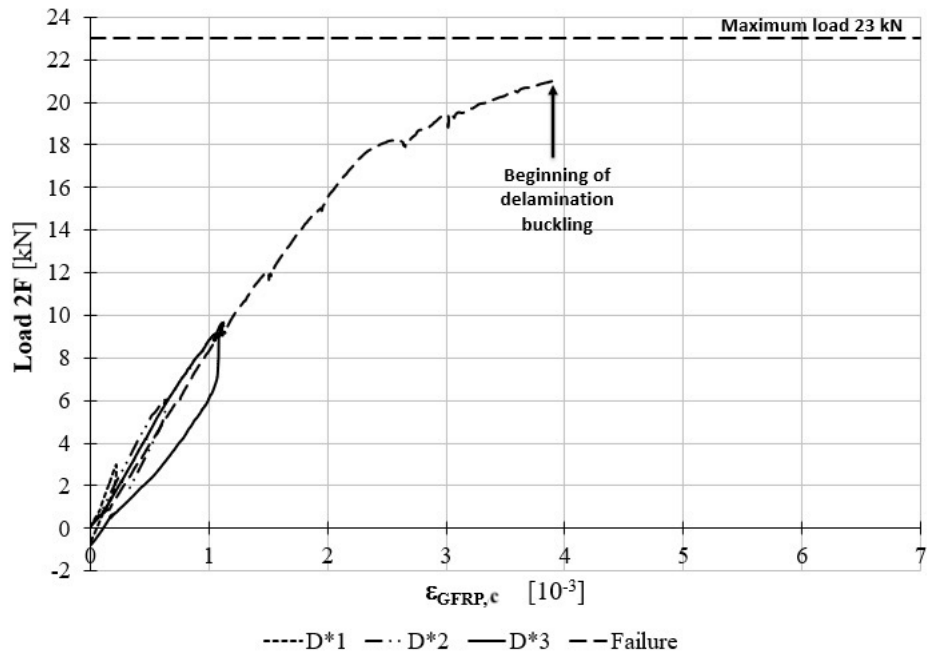


Figure 9 – Exp. diagram load, $2F$, vs strain of GFRP strip, $\epsilon_{GFRP,c}$ at the compressive side of beam A.

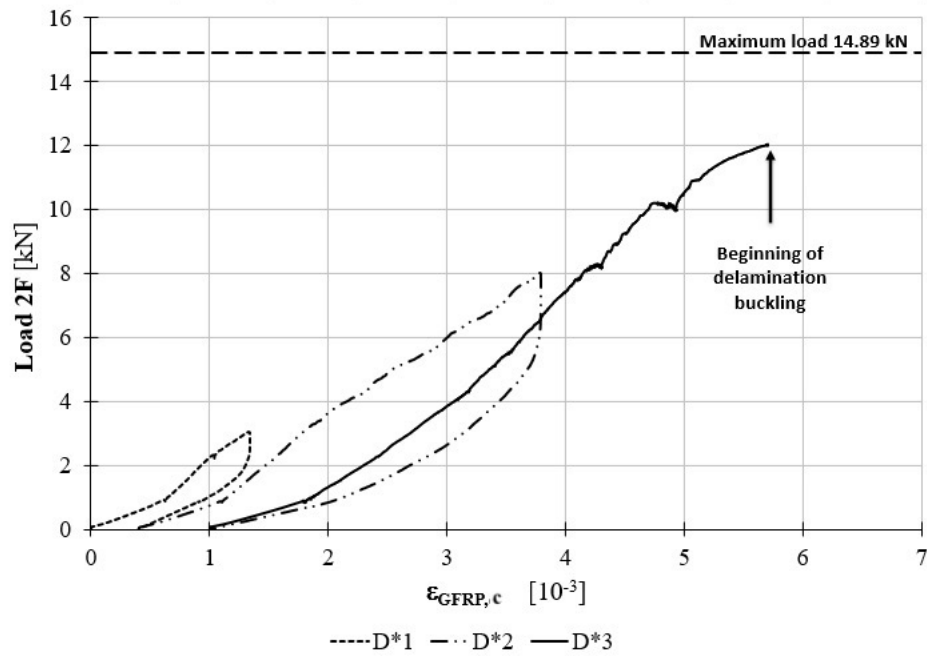


Figure 10 – Exp. diagram load, $2F$, vs strain of GFRP strip, $\epsilon_{GFRP,c}$, at the compressive side of beam B.

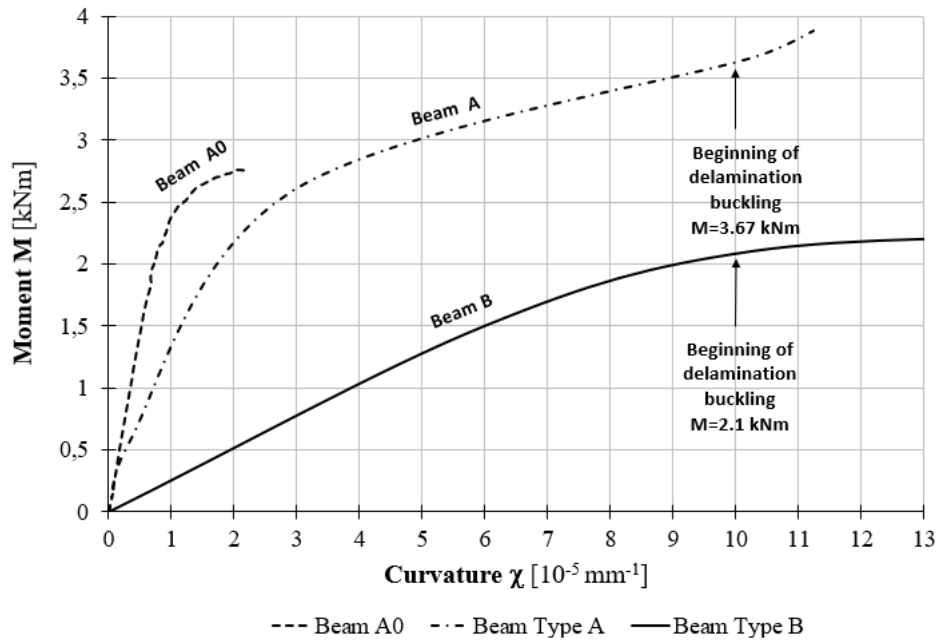


Figure 11 - Comparison between experimental moment, M , vs. curvature, χ , diagrams.

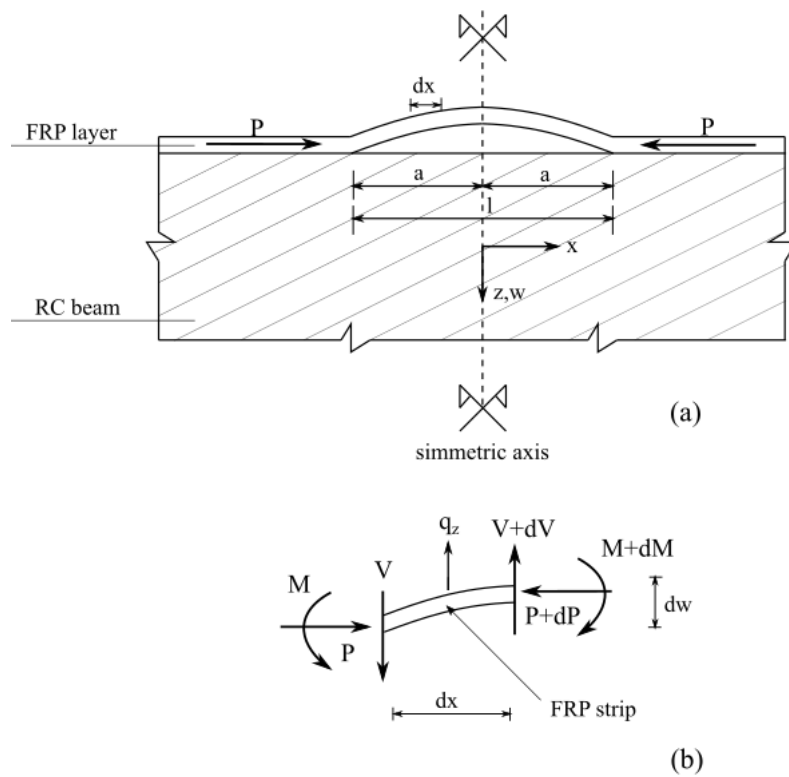


Figure 12 – (a) Local delamination buckling of FRP strip; (b) internal action.

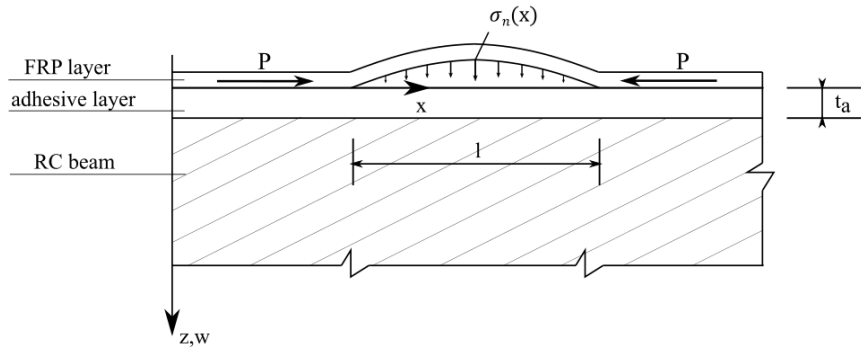


Figure 13 – Deflection of compressed FRP strip.

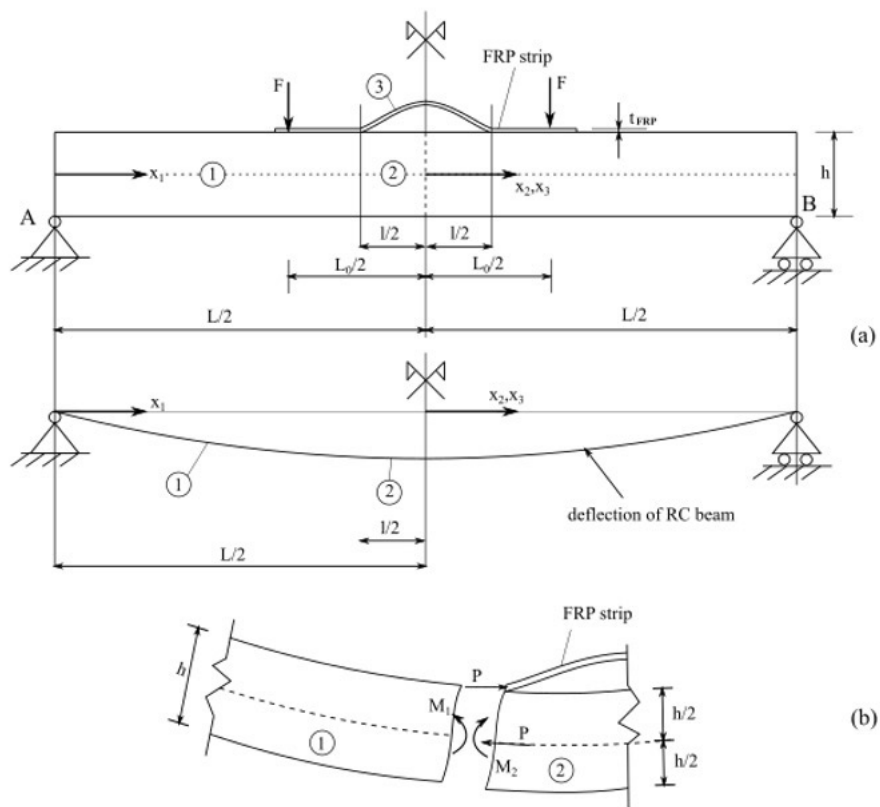


Figure 14 – (a) RC beam under bending experimental test; (b) RC beam with FRP delaminated.

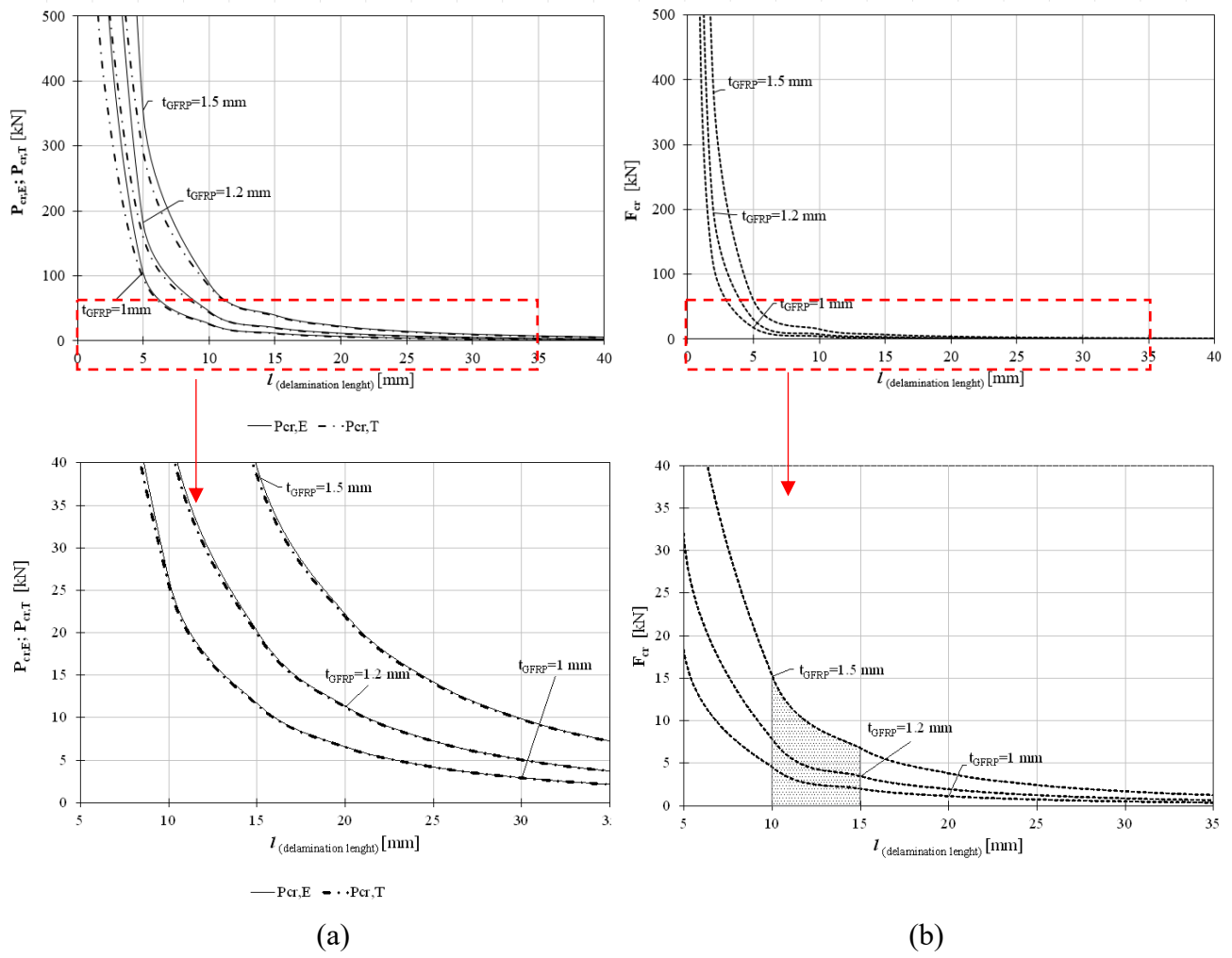


Figure 15 - (a) Theoretical diagrams $P_{cr,E}$, $P_{cr,T}$, vs delamination length, l and (b) theoretical diagrams F_{cr} , vs delamination length, l , for different values of GFRP thickness, t_{GFRP} , of strip.

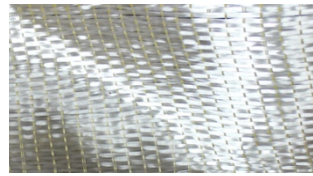
List of Tables:

- Table 1 Experimental data of RC beam models.
- Table 2 Experimental dimensions of GFRP specimens and results obtained by tensile tests.
- Table 3 Main experimental results for RC beam models under static bending test.
- Table 4 Theoretical values of normal stiffness of the adhesive, K_n , vs thickness of GFRP strip.

Table 1 – Experimental data of RC beam models.

Beam model	Width B [mm]	Height h [mm]	Length L [mm]	Compressive strength f_c [N/mm ²]	Young's modulus E_c [kN/mm ²]	Moment of inertia I [mm ⁴ ·10 ³]
A0	80	120	1100	18.38	28.43	11520
A	80	120	1100	24.9	31.45	11520
B	80	120	1100	18.38	28.43	11520

Table 2 – Experimental dimensions of GFRP specimens and results obtained by tensile tests.



1. FIDGLASS UNI 300 HT 73

Specimen	Measured thickness	Width	Cross section Area	Equivalent Area
	t_{GFRP} [mm]	b [mm]	A_{GFRP} [mm ²]	[mm ²]
TG1	1.17	14.38	16.82	5.18
TG2	1.22	15.12	18.45	5.44
Specimen	Tensile strength	Ultimate strain*	Density*	Experimental Modulus
	f_{GFRP} [N/mm ²]	ε_{GFRP} (%)	ρ (g/m ³)	E_{GFRP} [GPa]
TG1	1229.5	2.00	300	-
TG2	1317.1	2.00	300	64.0

[*] values declared by the manufacturer.

Table 3 – Main experimental results for RC beam models under static bending test.

Beam type A0						
Damage steps	Load $2F$	Moment	Strain at compressive concrete		Strain at tensile concrete	Curvature of midspan section
	[kN]	[kNm]	ϵ_c (%)		ϵ_{ct} (%)	χ [10^{-5} mm^{-1}]
D*1	3.00	0.53	0.24		0.01	0.21
D*2	8.00	1.40	0.65		0.08	0.62
D*3	12.00	2.10	0.91		0.09	0.83
Failure	15.77	2.76	-		-	-
Beam type A						
Damage steps	Load $2F$	Moment	Strain at compressive concrete	Strain at compressive GFRP strip	Strain at tensile GFRP strip	Curvature of midspan section
	[kN]	[kNm]	ϵ_c (%)	$\epsilon_{FRP,c}$ (%)	$\epsilon_{FRP,t}$ (%)	χ [10^{-5} mm^{-1}]
D*1	3.00	0.53	0.13	0.22	0.086	0.294
D*2	6.00	1.05	0.44	0.63	0.97	1.54
D*3	9.00	2.59	0.37	1.06	2.05	2.93
Failure	23	3.88	-	-	-	-
Beam type B						
Damage steps	Load $2F$	Moment	Strain at compressive concrete	Strain at compressive GFRP strip	Strain at tensile GFRP strip	Curvature of midspan section
	[kN]	[kNm]	ϵ_c (%)	$\epsilon_{FRP,c}$ (%)	$\epsilon_{FRP,t}$ (%)	χ [10^{-5} mm^{-1}]
D*1	4.00	0.53	-	1.19	1.51	2.25
D*2	8.00	1.40	-	3.78	3.32	5.92
D*3	12.00	2.10	-	5.69	6.62	10.25
Failure	14.89	2.61	3.87	-	-	-

Table 4 – Theoretical values of normal stiffness of the adhesive, K_n , vs thickness of GFRP strip.

Normal stiffness of the adhesive K_n [kN•mm ⁻³]								
Delamination length l [mm]	Thickness of GFRP strip t_{GFRP} [mm]							
	1.0	1.2	1.5	1.6	1.7	1.8	1.9	2.0
10	0.013	0.022	0.044	0.053	0.064	0.0756	0.0889	0.104
11	0.0088	0.015	0.03	0.036	0.043	0.0516	0.061	0.07
12	0.006	0.011	0.021	0.0256	0.0307	0.036	0.043	0.05
13	0.0045	0.0078	0.015	0.01859	0.0223	0.0265	0.031	0.036
14	0.0034	0.0058	0.011	0.0138	0.0166	0.0197	0.023	0.027
15	0.0026	0.0044	0.0086	0.0105	0.0126	0.015	0.017	0.0205